ISSN 0021-8944, Journal of Applied Mechanics and Technical Physics, 2021, Vol. 62, No. 6, pp. 991–1000. © Pleiades Publishing, Ltd., 2021.
Russian Text © M. Azadi Moghaddam, F. Kolahan.

OPTIMIZATION OF OXIDE-BASED ACTIVATING FLUX COMBINATION FORMULA IN ACTIVATED TUNGSTEN INERT GAS WELDING USING A HYBRID METHOD INCLUDING ARTIFICIAL NEURAL NETWORKS AND PARTICLE SWARM OPTIMIZATION

M. Azadi Moghaddam[a,*] and F. Kolahan[a]

UDC 621.791

Abstract: The effects of the most important process-adjusting variables (welding current and welding speed) and the percentage of the combination of TiO_2 and SiO_2 activating fluxes on the most important quality characteristics (weld bead width, depth of penetration, and aspect ratio of these parameters) in welding of AISI316L austenite stainless steel parts are considered. Artificial neural networks (ANN) are used to determine the relations between the input variables and output responses of the activated tungsten inert gas (A-TIG) welding process. To determine the proper ANN architecture (the proper number of hidden layers and their corresponding neurons/nodes), the particle swarm optimization (PSO) method is used. Experimental tests are conducted to evaluate the proposed procedure performance. Based on the results, the proposed method is found to be efficient in modeling and optimization of the A-TIG welding process.

Keywords: activated tungsten inert gas (A-TIG) welding process, response surface methodology (RSM), artificial neural network (ANN), particle swarm optimization (PSO) algorithm, and simulated annealing (SA) algorithm.

DOI: 10.1134/S0021894421060146

INTRODUCTION

Tungsten inert gas (TIG) welding, also known as gas tungsten arc welding (GTAW), is extensively employed to fabricate aluminum, magnesium, stainless steel, and titanium alloys due to its surface finish (spatter-free process) and high quality. Shallow penetration was investigated as a drawback of TIG welding of thick parts [1]. To tackle the problem of poor penetration in the TIG welding process, various procedures were introduced, including the use of activating fluxes (oxides, fluorides, and chlorides) prepared as a paste and coated onto the weld surface before the welding process starts. This procedure is called activated tungsten inert gas (A-TIG) welding [2, 3]. A-TIG welding is effectively employed for various materials, namely, titanium, aluminum, manganese, and stainless steel (including austenite and austenite duplex) alloys. Moreover, welding of dissimilar metals due to stabilizing the depth of penetration based on reversal of the Marangoni convection could be considered as another merit of A-TIG welding [4, 5].

When the thickness of the welded specimens exceeds 3 mm, a filler metal is needed to fill the welding gap between the specimens in C-TIG welding, whereas application of A-TIG welding allows steel parts (around 8 mm thick) to be fabricated using a single welding pass and even without using filler metals and edge preparation [6].

[a]Ferdowsi University of Mashhad, Mashhad, Iran; *masoudazadi888@gmail.com, kolahan@um.ac.ir. Translated from Prikladnaya Mekhanika i Tekhnicheskaya Fizika, Vol. 62, No. 6, pp. 119–129, November–December, 2021. Original article submitted June 16, 2020; revision submitted July 4, 2020; accepted for publication July 27, 2020.
*Corresponding author.

Vidyarthy et al. [1] investigated the effects of the activating fluxes on the microstructural and mechanical properties and on the corrosion behavior in welding of dissimilar AISI316L and P91 steel parts. The effect of the activating flux on the mechanical and microstructural properties of the TIG-welded Ti-6Al-4V titanium alloy specimens was studied by Ramkumar et al. [2]. Based on the results, the microstructural and mechanical properties of the weld were improved by using the activating flux. Furthermore, the mechanical properties were investigated by Zou et al. [3] in A-TIG welding of duplex stainless and ferrite steels and by Kulkarni et al. [4] in A-TIG welding of dissimilar materials (Inconel 800 and Inconel 600). The microstructural and mechanical properties of A-TIG welded P91 parts were studied in [5, 6]. The GTAW process was optimized by using the response surface methodology (RSM) in order to reach the largest possible depth of penetration [7].

In the above-cited papers, optimization of the process output responses was not performed. To the best of our knowledge, there are no studies in which modeling and optimization of the depth of penetration (DOP), weld bead width (WBW), and aspect ratio (AR) are considered simultaneously using the RSM-based design of experiments, modeling based on using artificial neural networks (ANN), and optimization techniques based on heuristic algorithms: simulated annealing (SA) and particle swarm optimization (PSO) algorithms.

As different activating fluxes produce different effects on the weld bead geometry and on the mechanical and metallurgical properties of the welded parts, the percentage of the activating fluxes is considered in the present study as a process input variable (in addition to the welding speed and current) and is optimized in such a way that the depth of penetration D increases, weld bead width W decreases, and a proper aspect ratio is achieved simultaneously.

In this study, based on the preliminary experimental tests carried out using the design of experiments (DOE) approach and the literature survey studied, three inputs parameters (welding current I, welding speed S, and percentage of activating fluxes F) were taken into account as adjusting parameters. According to the number of input variables and their predetermined levels, the most appropriate design matrix (central composite design (CCD) based on RSM) was considered. Next, the back propagation neural network (BPNN) was used to determine the relationships between the process input variables and output characteristics. Next, the PSO algorithm was applied to find the best BPNN architecture (number of hidden layers and nodes/neurons in each layer). Finally, the optimal values of the process input variables for multi-response optimization were determined using the PSO algorithm. The SA algorithm was used to check the adequacy of the PSO algorithm and avoid getting trapped in local minima.

1. EXPERIMENTAL SETUP AND MATERIALS USED

There are various variables affecting the A-TIG welding process; the most influential ones are the welding speed S, welding current I, and percentage of the activating fluxes F [1–3]. To determine possible ranges of each input variable of the welding process (Table 1), welding references were studied, and preliminary experiments were performed. The variable F varied in the interval 0–100%, the variable I varied in the interval 90–130 A, and the variable S varied in the interval 110–190 mm/s.

To carry out the experimental tests based on the CCD matrix proposed by the RSM, a DIGITIG 250 AC/DC welding machine was employed. Furthermore, in this study, argon (with 99.7% purity) was used as a shielding inert gas.

AISI316L stainless steel plates with dimensions of $100 \times 50 \times 5$ mm were considered as specimens. In this study, nano-oxide fluxes (TiO_2 and SiO_2) (99%, 20–30 nm, amorphous) were used as activating fluxes. The powder particle size was determined by using a FESEM microscope.

Table 1. Process input variables and their corresponding intervals and levels

Level F	F, %	I, A	S, mm/s
1	0–100	90	110
2	25–75	100	130
3	50–50	110	150
4	75–25	120	170
5	100–0	130	190

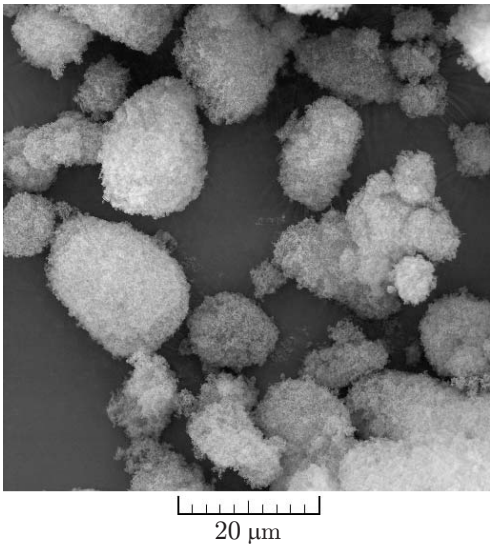

Fig. 1. Activating flux with SiO_2 and TiO_2 nanoparticles.

Figure 1 represents the FESEM results of the oxide-based activating fluxes, which confirmed the nanoscale claimed by the provider. Prior to welding process beginning, 20 g of the flux were mixed with 20 ml of the carrier solvent (methanol) using mechanical, magnetic, and ultrasonic mixers until a paste-like flux was obtained (approximately 20 min in each mixer) [1, 2]. Then, the paste-like flux was coated onto the specimen with a brush and dried.

The DOE method proposes a wide variety of different approaches, among which the RSM acts as a powerful tool. The RSM comprises various designs, including the central composite design (CCD) (spherical CCD, rotatable CCD, etc.), Box-Behnken design (BBD), and hybrid designs [8]. In this study, the L_{20} CCD matrix was used (Table 2). A random order in conducting experiments was used to increase the accuracy of the experiments. After welding, three types of responses (weld bead width W, depth of penetration D, and aspect ratio W/D were measured for each specimen (see Table 2).

Table 2. Experimental conditions based on CCD and corresponding measured output responses

Test No.	S, mm/s	I, A	F, %	D, mm	W, mm	W/D
1	130	120	25	5.755	7.693	1.337
2	150	110	50	5.041	7.905	1.568
3	170	100	75	5.367	7.224	1.346
4	170	100	25	3.142	9.466	3.013
5	150	110	50	4.711	7.617	1.617
6	150	130	50	6.827	7.703	1.128
7	170	120	25	3.920	8.425	2.149
8	170	120	75	5.524	5.923	1.072
9	130	100	25	4.873	8.125	1.667
10	150	110	50	4.321	7.920	1.833
11	150	110	50	4.850	7.510	1.548
12	130	100	75	6.356	6.676	1.051
13	150	110	50	4.950	7.847	1.585
14	150	110	100	6.124	5.604	0.915
15	110	110	50	6.254	6.393	1.022
16	150	90	50	4.610	7.778	1.687
17	150	110	50	4.906	7.803	1.591
18	130	120	75	7.894	6.910	0.875
19	150	110	0	3.133	9.985	3.187
20	190	110	50	3.850	7.460	1.938

Two cuts were made on the surface of each specimen to measure D, W, and W/D. To determine D and W accurately, the cut faces were polished smoothly and etched. The surface images were taken by an optical microscope. The values of D and W were determined by using the MIP software (Fig. 2).

To relate the process input variables and output responses, the following regression equations are solved for D, W, and W/D:

$$D = 24.19 + 0.033\,58\,F - 0.381\,C + 0.000\,230\,S^2 - 0.000\,960\,SC + 0.002\,608\,C^2,$$

$$W = -28.83 + 0.0549\,F + 0.3483\,S + 0.1842\,C - 0.000\,628\,FS - 0.000\,526\,S^2 - 0.001\,340\,SC,$$

$$W/D = -15.39 + 0.1125\,S + 0.1634\,C + 0.000\,155\,F^2 - 0.000\,448\,FS + \\ + 0.000\,280\,FC - 0.000\,109\,S^2 - 0.000\,395\,SC - 0.000\,615\,C^2.$$

2. BACK PROPAGATION NEURAL NETWORK

ANNs are extensively employed as a nonlinear and parallel processing system in order to relate a set of input-output parameters. They consist of a set of connected processing units called neurons/nodes organized in each layer (input, hidden, and output layers) by connections that connect the nodes. Each input variable (defined as x_i) is assigned a weight w_i indicating the portion of the input variable transferred to the neuron for processing. Furthermore, b is the bias (systematic error), and y is the output signal. The received signal

$$v = \sum_{i=1}^{N} x_i w_i + b$$

is transferred by the using the function f into the output signal ($y = f(v)$) [9].

Various ANN structures were proposed among which the multi-layer perceptron (MLP) was extensively used due to its ability to solve nonlinear separable/continuous problems. The MLP contains an input layer, one or more hidden layer/s, and an output layer. In the training stage, a supervised way is used to determine the biases and weights, based a set of input-output data pairs, which allows the MLP to learn the relationships between the input-output parameters. In the BPNN, an algorithm (back propagation) in which the error of each input-output pair in the MLP is calculated and is then transferred from the last (output) to the first (input) layer, where the biases and weights of the MLP network are adjusted. The details in this regard are well documented in [9, 10].

Commonly, the architecture of ANN models is determined using the trial and error procedure. In this study, however, the PSO algorithm was used to determine the proper BPNN architecture. The number of hidden layers was varied from 1 to 3; hence, a $3{-}n_1{-}n_2{-}n_3{-}3$ structure was constructed, where n_1, n_2, and n_3 are the numbers of neurons/ nodes in the 1st to 3rd hidden layer. The training stage acts as a way to find the proper weights and architecture that ensure the minimum error between the desired (or predetermined) and predicted results.

3. PROBLEM DEFINITION

In this study, a low value of W, a high value of D, and a desired value of W/D had to be reached simultaneously.

Therefore, the study of the process multi-responses reduces to finding the minimum of the function

$$f(F, I, S) = w_1 D - w_2 W,$$

where $1.0 < W/D < 1.4$, $0 < F < 100\%$, 90 A $< I <$ 130 A, and 110 mm/s $< S <$ 190 mm/s; w_1 and w_2 are the weights determining the contributions of D and W, respectively. According to the literature survey, the optimal range of the aspect ratio W/D is $[1.0; 1.4]$ [11]. For W/D values within this range, the probability of cracking in the case of weld solidification is fairly low.

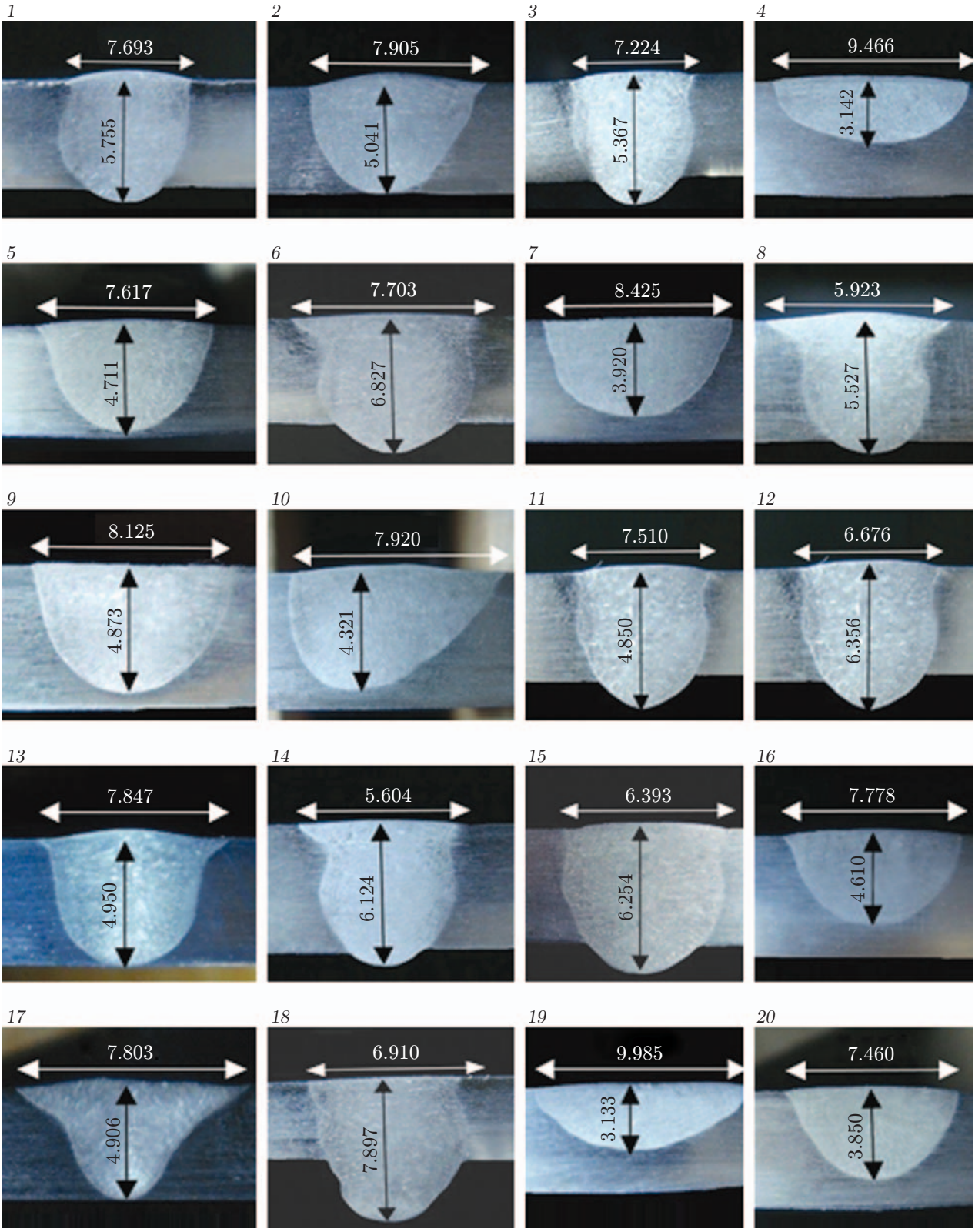

Fig. 2. Cross-sectional profiles obtained by A-TIG welding in experiments 1–20.

4. HEURISTIC ALGORITHMS

Various heuristic algorithms were proposed to search for an optimal range of the input parameters that ensure a required result at the output. The most popular methods are the particle swarm optimization and simulated annealing methods. Easy programming (few input parameters to adjust) and fast convergence are the major merits of the PSO algorithm. However, in a high-dimensional space, falling into local minimum traps may be considered as a weakness of the PSO algorithm. The SA mechanism can avoid getting trapped into local minima; moreover, the SA algorithm has several advantages over other algorithms [12].

In this study, the PSO and SA algorithms were employed as heuristic algorithms to optimize the A-TIG welding process variables in order to achieve the maximum DOP, the minimum WBW, and the proper value of the aspect ratio. In this study, the PSO method was used twice to determine the most appropriate BPNN architecture and to optimize the process measures. Next, the SA algorithm was used to evaluate the PSO performance. Furthermore, a set of validation experiments was conducted in order to confirm the proposed approach.

4.1. Simulated Annealing Algorithm

Various methods are used to select the most appropriate values of the process input parameters that ensure reaching the desired output characteristics [12]. The mechanism of the SA algorithm is defined as follows. First, an acceptable solution (response) space is defined, and an initial random solution in this space is generated. Next, the objective function of the new solution C_1 is computed and compared with the objective function of the current solution C_0. The transition to the new solution occurs either when the new solution has a better value of the objective function or when the probability function

$$P_r = \mathrm{e}^{-\Delta C/T_k}$$

is greater than a randomly generated number between 0 and 1.

Let T_k be the temperature in the physical annealing process [12]. The equation

$$T_{k+1} = \alpha T_k, \quad k = 0, 1, \ldots, \qquad 0{,}9 \leqslant \alpha < 1{,}0$$

is used as to reduce the temperature at each iteration.

The cooling rate depends on the parameter α. At the first iterations of the SA method, the cooling rate may fail to decrease (and even may increase) due to high temperature. Nonetheless, the temperature does decrease as the algorithm proceeds, which helps the algorithm avoid being trapped in local minima.

The algorithm procedure steps are described below.

Step 1. The temperature T_0, cooling rate $0 < r < 1$, and termination criterion (number of iterations $k = 1, \ldots, K$) are determined. The random initial solution (current solution c) is generated and evaluated.

Step 2. A new neighboring solution m close to the current solution is generated and evaluated by means of varying the current solution.

Step 3. The new solution is accepted as the current solution if the following conditions are satisfied:

(a) the objective function of the new solution $E(m)$ is better than that of the current solution $E(c)$;

(b) the value of the acceptance probability function $\mathrm{e}^{(f(m)-f(c))/T_k}$ is greater than a uniformly generated random number in the interval $[0, 1]$.

Step 4. The termination criterion is checked, the temperature parameter is updated ($T_k = rT_{k-1}$), and the calculation returns to Step 2.

4.2. Particle Swarm Optimization Algorithm

The PSO method is a heuristic algorithm proposed in [13]. It begins with a population of random solutions, which is updated and searched for optimal ones. The current optimal solutions are followed by random solutions (known as particles) in the problem space. The solution (particle) updating is performed with the equations [13]

$$V_{i+1} = wV_i + c_1 r_i(\mathrm{pB}_i - X_i) + c_2 r_i(\mathrm{gB}_i - X_i); \tag{1}$$

$$X_{i+1} = X_i + V_{i+1}, \tag{2}$$

where the velocity V_{i+1} of each particle is determined based on its previous velocity V_i, global best solution (pB), and particle location (gB). Equation (2) was used for updating the particle position [13]. The terms r_1 and r_2 are two random numbers generated independently in the range $[0, 1]$. There are acceleration constants c_1 and c_2, which pull each particle (solution) toward the pB and gB positions. The inertia weight w acts as an important parameter in the PSO algorithm convergence behavior. In order to explore the solution space globally, a large value of w is required, while a small value of w is sufficient to explore nearby regions of the space [13].

Based on the literature survey, the BPNN architecture (number of hidden layers and number of nodes in hidden layers) in most studies was determined by the trial and error method. In this study, the PSO algorithm was employed to determine the PBNN architecture. Furthermore, the optimization of the proposed BPNN model was carried out using the PSO algorithm. The adjusting parameters used for the SA and PSO algorithms [13] are the population of 50, the learning factor $c_1 = c_2 = 2$, and the number of iteration performed equal to 30 in the PSO algorithm, and the temperature reduction rate of 0.91, the processing time of 30 s, and the initial temperature of 700 in the SA algorithm.

The proposed hybrid ANN-PSO model is presented in Fig. 3.

RESULTS AND DISCUSSION

The value of the weights w_1 and w_2 for D and W was chosen in the present study to be 0.5. The optimization procedure was used for two conditions. In the first variant, the weld bead geometry was not restricted. In the second variant, a dimensional restriction was imposed to the maximum DOP value (5 mm), and the value of the W/D ratio had to be in the interval $[1.0; 1.4]$. Figure 4 illustrates the weld cross section obtained in the case of optimization under the second condition. Based on the nature of the PSO algorithm, its convergence is faster than that ensured by the SA algorithm. Furthermore, as the PSO drawback is falling into local minimum traps, its performance could be better checked against the results obtained by other algorithms. In this paper, the performance of the PSO algorithm was checked with the SA algorithm performance. The convergence of the PSO and SA algorithms is shown in Fig. 5.

Table 3 represents the results of PSO and SA optimization of the weld parameters. The difference in the results is smaller than $\Delta = 2.1\%$.

The ultimate tensile stress (UTS) test was performed under the optimized conditions (for both TIG and A-TIG welding processes). The corresponding values are 616 and 638 MPa, respectively.

CONCLUSIONS

Modeling and optimization of the A-TIG welding process for AISI316L austenite stainless steel parts were performed. The weld bead geometry and the percentage of the activating fluxes were optimized. First, the CCD was used in the RSM to determine the experimental design matrix required for data acquisition, modeling, and optimization purposes. Next, the DOP and WBW values were measured using the MIP software, and the aspect ratio of these parameters was computed. Then, the BPNN was employed to establish the relations between the process input variables (welding speed, welding current, and percentage of activating fluxes) and output responses (depth of penetration, weld bead width, and aspect ratio). Moreover, in order to determine the proper BPNN architecture, the PSO algorithm was applied. Then, the PSO algorithm was used again to optimize the proposed BPNN model. Using the proposed hybrid BPNN-PSO approach, the process input variables were optimized: 190 mm/s for the welding speed and 128 A for the welding current. The optimal percentage of the activating fluxes was found to be 71% for SiO_2 and 29% for TiO_2. Optimal parameters of welding ensure the maximum depth of penetration and the minimum weld bead width for a given ratio of these parameters. The result of the proposed optimization procedure shows that the proposed method can precisely simulate and optimize the A-TIG welding process.

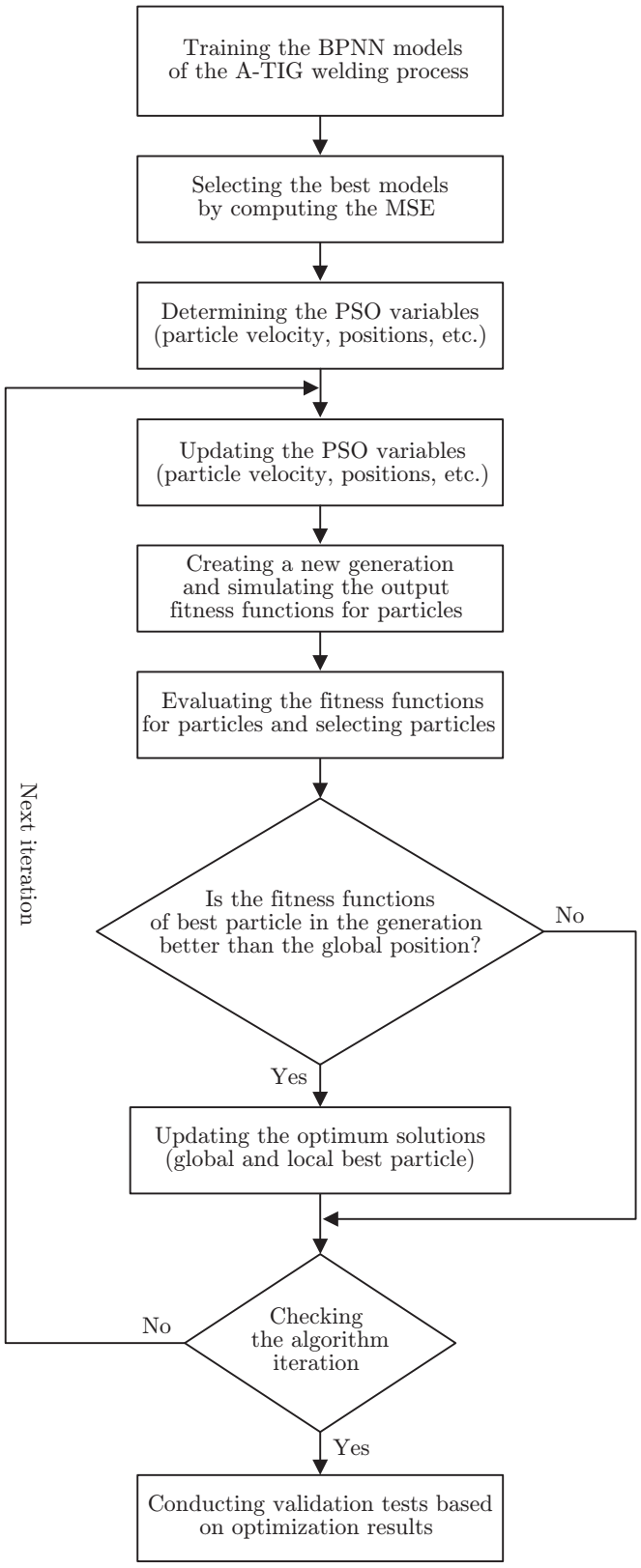

Fig. 3. Illustration of the proposed hybrid ANN-PSO method.

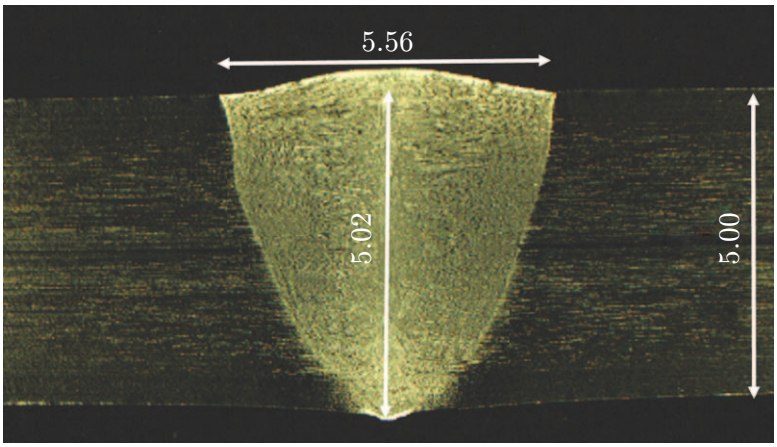

Fig. 4. Depth of penetration and weld bead width obtained after optimization.

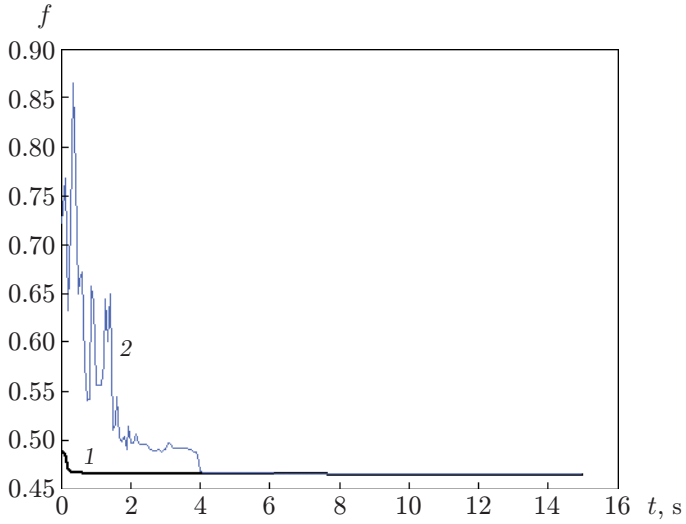

Fig. 5. Convergence of the heuristic methods: particle swarm optimization (*1*) and simulated annealing (*2*).

Table 3. Optimal parameters of A-TIG welding and their experimental values

Optimization variant	Method	F, %	S, mm/s	I, A	Output response	Prediction	Experiment	Δ, %
with weld bead geometry restriction	SA	60	190	129	D	4.99 mm	5.02 mm	0.7
	PSO	71	190	128	D	4.98 mm	5.02 mm	0.8
	SA	60	190	129	W	5.49 mm	5.56 mm	1.3
	PSO	71	190	128	W	5.48 mm	5.56 mm	1.4
	PSO	60	190	129	W/D	1.10	1.11	0.9
	SA	71	190	128	W/D	1.10	1.11	0.9
without weld bead geometry restriction	SA	99	110	129	D	9.54 mm	9.66 mm	1.2
	PSO	100	110	130	D	9.55 mm	9.66 mm	1.1
	SA	99	110	129	W	9.64 mm	9.85 mm	2.1
	PSO	100	110	130	W	9.65 mm	9.85 mm	2.1
	PSO	99	110	129	W/D	1.01	1.02	1.0
	SA	100	110	130	W/D	1.01	1.02	1.0

REFERENCES

1. R. S. Vidyarthy, A. Kulkarni, and D. K. Dwivedi, "Study of Microstructure and Mechanical Property Relationships of A-TIG Welded P91-316L Dissimilar Steel Joint," Materials Sci. Engng. A **695** (5), 249–257 (2017).
2. K. D. Ramkumar, V. Varma, M. Prasad, and N. D. Rajan, "Effect of Activated Flux on Penetration Depth, Microstructure and Mechanical Properties of Ti-6Al-4V TIG Welds," J. Materials Process. Technol. **261** (5), 233–241 (2018).
3. Y. Zou, R. Ueji, and H. Fujii, "Mechanical Properties of Advanced Active-TIG Welded Duplex Stainless Steel and Ferrite Steel," Materials Sci. Engng. A **620** (6), 140–148 (2015).
4. A. Kulkarni, D. K. Dwivedi, and M. Vasudevan, "Dissimilar Metal Welding of P91 Steel-AISI 316L SS with Incoloy 800 and Inconel 600 Interlayers by using Activated TIG Welding Process and its Effect on the Microstructure and Mechanical Properties," J. Materials Process. Technol. **274** (3), 116–128 (2019).
5. R. S. Vidyarthy and D. K. Dwivedi, "Microstructural and Mechanical Properties Assessment of the P91 A-TIG Weld Joints," J. Manufactur. Process **31** (12), 523–535 (2018).
6. K. H. Dhandha and V. J. Badheka, "Effect of Activating Fluxes on Weld Bead Morphology of P91 Steel Bead-on-Plate Welds by Flux Assisted Tungsten Inert Gas Welding Process," Materials Manufactur. Process. **17** (4), 48–57 (2015).
7. R. Pamnani, M. Vasudevan, P. Vasantharaja, and T. Jayakumar, "Optimization of A-GTAW Welding Parameters for Naval Steel (DMR 249 A) by Design of Experiments Approach," Proc. Inst. Mech. Engrs. Pt L: J. Materials Design Appl. **34** (8), 1–12 (2015).
8. S. Tathgir and A. Bhattacharya, "Activated-TIG Welding of Different Steels: Influence of Various Flux and Shielding Gas," Materials Manufactur. Process. **31** (3), 335–342 (2015).
9. H. Sahin and B. Topal, "Impact of Information Technology on Business Performance: Integrated Structural Equation Modelling and Artificial Neural Network Approach," Sci. Iran. B **25** (6), 1272–1280 (2018).
10. M. Kurtulmus and A. Kiraz, "Artificial Neural Network Modelling for Polyethylene FSSW Parameters," Sci. Iran. B **25** (1), 1266–1271 (2018).
11. G. Neville, *Why do Welds Crack?* TWI Bull. 1991. Mar./Apr. P. 1–8.
12. M. A. Ayubi Rad and M. S. Ayubi Rad, "Comparison of Artificial Neural Network and Coupled Simulated Annealing Based Least Square Support Vector Regression Models for Prediction of Compressive Strength of High-Performance Concrete," Sci. Iran. A **24** (3), 487–496 (2017).
13. M. Azadi Moghaddam, R. Golmezergi, and F. Kolahan, "Multi-Variable Measurements and Optimization of GMAW Parameters for API-X42 Steel Alloy using a Hybrid BPNN–PSO Approach," Measurement. **92** (13), 279–287 (2016).